Synthesis of high-modulus thermoset PUs of PCL-PTMG/CNW Biomaterials with different Soft Domain Architecture and Composition for high Shape Memory Performance

Elahe Aboueimehrizi
Amirkabir University of Technology Department of Polymer Engineering and Color Technology
Mohammad Amin Makaremy
Amirkabir University of Technology Department of Polymer Engineering and Color Technology
Sina Bazrpash
Amirkabir University of Technology Department of Polymer Engineering and Color Technology
Fatemeh Noormohammadi
Amirkabir University of Technology Department of Polymer Engineering and Color Technology
Yasaman Rahimi Darestani
Amirkabir University of Technology Department of Polymer Engineering and Color Technology
Mohammad Nourany (m.nourany@aut.ac.ir)
Amirkabir University of Technology Department of Polymer Engineering and Color Technology

Research Article

Keywords: Cellulose Nanowhisker, Thermoset Polyurethane, Thermomechanical Properties, Shape Memory Performance

Posted Date: April 13th, 2022

DOI: https://doi.org/10.21203/rs.3.rs-1439700/v1

Abstract

In this research work, a group of thermoset polyurethane (tPU) nanocomposites were synthesized. Poly(ε-caprolactone) (PCL_{2000}), Poly (tetramethylene glycol) ($PTMG_{2000}$), and different architecture and compositions of PCL and PTMG were used as diols. Cellulose nanowhisker (CNW), with 1.0 wt% content, was used to cross-link the prepolymers and to produce high-modulus specimens for high shape memory performance. The analyses of crystallization showed that thermal stability of the PTMG and PCL crystallites decreases upon block copolymerization, blending and incorporation of the block copolymer into the blend (about 10°C decrease). Cross-linking of the prepolymers using CNW has also reduced the crystallites' thermal stability to a large extent (about 50°C decrease). The results of the Dynamic Mechanical Thermal Analysis (DMTA) also showed that the thermoset PUs have a large elastic modulus at above room temperature (higher than 10 MPa) and very small tanδ height (below 0.15), which was attributed to its semi-crystalline nature and presence of CNW with high elastic modulus (110–220 GPa). The thermomechanical behavior of the tPUs proved to be ideal for acquiring high shape memory performance. The tPUs have also proved to be highly biocompatible.

Highlights

Synthesis of thermoset PU nanocomposites of CNW with high elastic modulus;

Prohibited clustering of CNWs (1.0 wt% content);

The change in soft segments' architecture affects Young's modulus;

Intense decline of soft segments' crystallization;

Wide tanδ peak and T_g transition allowed for tuning shape fixity;

Obtaining high shape memory performance due to high elastic nature of the PUs.

1. Introduction

Cellulose nanowhisker (CNW) is a rod-like crystalline nanoparticle, which has been the focus of numerous researches in the last decade (Lu & Hsieh, 2010). CNWs are extracted from natural resources including cotton, wood, rice straw, and other cellulose-rich plants (George & Sabapathi, 2015), (Roman et al., 2009). Different extraction procedures were developed to isolate CNWs from their raw materials including acid-hydrolysis, oxidization method, ionic liquid and enzymatic hydrolysis (Trache et al., 2017), (Vanderfleet & Cranston, 2021). Each of these four main procedures have their own advantages and disadvantages. However, regarding the cost and time of the extraction process, acid-hydrolysis was considered as the main choice available for efficient extraction (Mariano et al., 2014). Cotton was considered as the main renewable resource of CNWs (H. Du et al., 2019; Xie et al., 2018). The CNWs isolated from cotton by acid-hydrolysis had a crystallinity of 79–83%, an yield in the range of 57–69% with a diameter and length of

9–19 nm and 157–290 nm, respectively (Mu et al., 2019; Reid et al., 2017). CNWs have abundant -OH groups, which can be used for further chemical or physical modification (Roman et al., 2009; Tingaut et al., 2012).

CNW is considered a highly elastic nanorod, with an elastic modulus in the range of $\approx$ 110–220 GPa, and upon ideal dispersion in polymer matrices, they can act as an efficient mediator to transfer energy in the direction of applied force (Domingues et al., 2014; Lahiji et al., 2010; Tang et al., 2017). In the field of polymer nanocomposites, CNWs have been used as a filler to improve the mechanical properties of the matrix (SaifulAzry et al., 2021). However, its tendency towards clustering due to its hydrophilic nature has limited its application in most of hydrophobic polymers and further surface modifications were required (Park et al., 2013), (Pei et al., 2021). The cost and efficiency of the surface modification and its impact on the thermomechanical properties of the final nanocomposites has itself been a bigger challenge and drawback. According to the literature, nanocomposites of thermoplastic polyurethanes (TPUs) and CNWs have shown an improvement in mechanical properties including Young's modulus (Fortunati et al., 2017; Prataviera et al., 2018; Rueda et al., 2013). Despite numerous researches in this field, application of CNWs as an active agent in the field of thermoset polymers is limited. Their role as a cross-linking agent and their impact on the thermomechanical properties of the final thermoset polymer nanocomposites has not been fully investigated.

According to the literature, CNWs have been used as a nano-filler for cross-linking prepolymers of semi-crystalline soft segments. The results have shown significant changes in crystallization of the soft segments and a reduction in sensitivity of elastic modulus to temperature after the glass transition temperature (T_g) in the plateau region. Jafari et al. have synthesized thermoplastic and thermoset PUs based on semi-crystalline poly(ε-caprolactone) (PCL)/polyethylene glycol (PEG) polyols and CNWs (Jafari et al., 2020). The results indicated an intense decline in crystallization degree (X_c) and temperature (T_c) for the thermoset PUs compared to the thermoplastic PUs. The structural changes have reduced the temperature dependency of the elastic modulus at plateau region while having higher elastic modulus, which was attributed to the presence of CNWs. In another work, Noormohammadi et al. also reported that in a thermoset PU based on PCL_{500}-PEG_y-PCL_{500} block copolymers, for CNW contents higher than 0.50 wt.%, the crystallization temperature shows a slight increase, which was attributed to the nucleating role of the excessive and free CNWs in the PEG phase (Noormohammadi et al., 2021b). According to similar works, the thermoset PUs of semi-crystalline polyols and CNWs have shown a reduction in chain dynamics and an increase in elastic modulus at temperatures above T_g. This property has rendered the PUs to have high shape memory performance (SMP) and superior mechanical properties compared to TPUs (Khadivi et al., 2019; Liu et al., 2015; Mi et al., 2018; Nourany et al., 2021; Ranjbar et al., 2021). Lack of a consistent experimental data on the relation between the microstructure of semi-crystalline low molecular weight (M_w) (co)polymers or polymer blends and their crystallization processes makes it hard to correlate the changes in the macroscopic properties of thermoset PU/CNW nanocomposites to their microstructure.

Regarding TPUs and thermoset PUs, they possess inherent thermal shape memory performance (Jiu et al., 2016; Joo et al., 2018; Shirole et al., 2018). A type of linear and thermoset polymers that can be thermally programmed through different heating and cooling cycles to undergo a reversible shape switching process between a permanent shape (L_1) and a strain-induced temporary shape (L_2). In a thermally programmable polymer there exists two main characteristic temperatures: switching temperature (T_s) and recovery temperature (T_r); and there exists two structural components: switching component (SC) and permanent component (PC) (Joo et al., 2018; Kausar, 2019; Y. Wang et al., 2018). In a thermoplastic polyurethane (TPU) system, the hard domains play the role of the PC. In TPUs, the physical cross-link nature of the hard domains prohibits the slippage of the chains of SC (Cao & Jana, 2007; Urbina et al., 2019; Y.-J. Wang et al., 2018). The curing process condition, including time and temperature, and the nature of hard segments would impact the ability of the hard segments to form segregated domains to reduce the possible hard segment- soft segment mixing. As a result, the size of the hard domains would be a function of the process conditions and chemical structure (Choi et al., 2012; Kausar, 2019). However, for a thermoset PU nanocomposite, the possibility of hard segment- soft segment mixing is eliminated and the final shape recovery improves to a large degree (Jiu et al., 2016). In a thermoset in-situ CNW-PU structure, the soft domain plays the role of SC, and the cross-link points, formed by the covalent bonding of urethane linkages and the CNWs, act as the PC (Jafari et al., 2020; Noormohammadi et al., 2021a; Ranjbar et al., 2021).

In this work, different microstructures of polyols were prepared using PCL and poly(tetramethylene glycol) (PTMG). The polyols were composed of neat PCL and PTMG, with molecular weights of 2000 g/mol, their 50:50 w:w blends, the tri-block of PCL_{1000}-$PTMG_{2000}$-PCL_{1000} and the 100:50 w:w ratio of the blend and the block copolymer. Their crystallization behavior was studied. These specimens were further used to prepare thermoset PU/CNW nanocomposites and their crystallization and dynamic behavior was also studied. The mechanical properties, the shape memory performance of the thermoset PUs and the impact of the change in elastic modulus on shape fixity and recovery was thoroughly investigated. The cytocompatibility of the thermoset PUs was studied to evaluate their potential for biomedical applications.

2. Experimental

2.1. Materials

Poly(ε-caprolactone) with molecular weight of 2000 D, Hexamethylene diisocyanate (HDI), Stannous Octoate ($Sn(Oct)_2$), Dibutyl tindilaurate were purchased from Sigma and were used as received. Dimethylformamide (DMF, Sigma), Sulfuric acid (98%, sigma) were also used as received. Refined cotton (Iran, Golestan) was used as the source for extraction of cellulose nanocrystals. Poly(tetramethylene glycol)-diol (Mitsubishi chemical co.) with a molecular weight (Mw) of 2000 D ($PTMG_{2000}$). DMEM and FBS (Gibco, UK), and penicillin/ streptomycin (Sigma). Culture plates and flasks (United Scientific F1004 Plastic Well Plate).

2.2. CNW Extraction

The CNW extraction from purified cotton is fully described in our previous work (Noormohammadi et al., 2021a). Here, we describe the procedure in brief. The sulfuric acid (98%) hydrolysis procedure was used for hydrolysis of cotton. 5 gr cotton and 100 ml acid solution (50 ml: 50 ml) was used for the hydrolysis procedure. The final suspension was centrifuged at 5000 rpm to extract the CNWs. Dialysis tube was used for increasing the pH of the CNWs to a range of 6.5-7.0. The surface-charge neutralized CNWs were further freeze-dried.

2.3. Block Copolymer Synthesis

The PCL_{1000}-$PTMG_{2000}$-PCL_{1000} block copolymer (Block 1:1) was synthesized using a pseudo-anionic bulk polymerization at 120°C. Stannous Octoate ($Sn(Oct)_2$) with a ratio of 0.2 mol% relative to $PTMG_{2000}$ was used as the catalyst. In the first step of the polymerization, 10 gr of PTMG with a molecular weight of 2000 D was added to a 50 ml round bottom 3-neck flask and heated to 120°C. Then, vacuum was applied to the melt to remove moisture and possible contamination. $Sn(Oct)_2$ was added to the flask. ε-caprolactone monomer (5.3 ml) was added to the flask and the flask was then sealed and the reaction was kept to proceed for 24 hours. The termination phase was performed using 5 ml solution of distilled water and a few droplets of 37% HCl. The final copolymer was precipitated in cold ether solvent. The efficiency of the polymerization was 94.6% and the resulted of Gel Permeation Chromatography showed that the final block copolymer possessed a number-averaged molecular weight of 4127 D with a PDI of 1.22.

2.4. Thermoset Polyurethane Synthesis

Table 1 provides the formulation recipe for synthesis of the thermoset PU/CNW nanocomposites. The molar ratio of HDI to each polyol was kept at 3:1. CNW content was 1.0 wt% relative to the prepolymer.

Table 1
The formulation recipe for synthesis of the thermoset PU synthesis.

Specimen	PCL_{2000} (gr)	$PTMG_{2000}$ (gr)	Block 1:1 (gr)	HDI (gr)	CNW (gr)
PCL-tPU	12	0	0	3.02	0.150
PTMG-tPU	0	12	0	3.02	0.150
Block 1:1-tPU	0	0	12	1.51	0.135
Blend-tPU	6	6	0	3.02	0.150
Mixture-tPU	4	4	4	2.52	0.145

The synthesis procedure is as follows: 1) Weighting the polyol(s) and adding them into the 3-necked bottom round flask; 2) heating and stirring the polyol(s) at 80°C and 250 rpm; 3) using vacuum for 15 minutes to eliminate the possible moisture and then, applying a continuous dry nitrogen purge; 4) adding

the PU catalysis solution, Dibutyl tin dilaurate in DMF, to the polyol(s) using a syringe; 5) dropwise addition of HDI to the reaction media and allowing the reaction to proceed for 2 hours to ensure complete conversion of diols into prepolymers; 6) adding the pre-sonicated CNW in DMF suspension to the flask; 7) allowing for the reaction to proceed for 30 minutes and then pouring the highly viscose solution into Teflon mold; finally, 8) putting the Teflon mold in oven at 70°C for 24 hours.

2.5. Cross-link Density and Degree Measurement

The equilibrium swelling test was used for measuring the cross-link density (CLD) of the thermoset PU/CNW nanocomposites. Three samples of each specimen with dimensions of 1 cm × 1 cm × 1 mm were cut and then immersed into a glass containing toluene and the result for each specimen was averaged over three. The samples were kept in the solvent for 72 hours at room conditions. The sealed glass containers were placed on a shaker to ensure dissolution of unreacted polyols into the solvent. The final stable weight of the swollen samples was selected as the equilibrium swelling weight (ESW). The thermodynamically developed Flory- Rehner equation was applied to measure the CLD.

$$\upsilon = \frac{-[\ln(1-V_r)+V_r+\chi V_r^2]}{V_0(V_r^{\frac{1}{3}}-0.5V_r)} \quad \text{Eq. 1,}$$

The parameters of υ, V_0, χ, and V_r represent the CLD, solvent molar-volume, polymer-solvent interaction parameter, volume fraction of the swollen thermoset PU/CNW nanocomposite. The cross-link degree or gel content of the specimens is measured using a Soxhlet extractor. Again, three samples of each specimen with dimensions of 1 cm × 1 cm × 1 mm were cut and placed into the Soxhlet and Toluene was used as the solvent. The siphon tube would create a flow to remove the dissolved polyols and procedure proceeded for 24 hours. The final dry-weight of the specimens was measured and divided by the original weight to get the gel fraction.

2.6. Shape Memory Procedure

The shape memory performance analysis of the thermoset PU specimens was performed through two different procedures. In the first procedure, the specimens with 2.5 × 1 × 0.1 cm^3 dimensions were bend over and fixed using a metal clamp. Then, the specimens were immediately put into liquid nitrogen for 5 minutes. Allowing for more freezing process time leads to brittleness and fracture of the specimens. In the next step, the specimens were put at room temperature and the clamp was removed. The camera was set to take pictures of the specimens every 15 seconds to follow the shape recovery process. The second procedure was to use a DMA instrument working in tension mode. The specimens' dimension was 2 × 0.5 × 0.1 cm^3. The thermal programming procedure was as follows: A) increasing temperature to 37.5°C; B) Applying a 30 N dynamic force to stretch the specimens; C) Decreasing temperature to -25°C; D) Removing the force; E) Increasing the temperature to 37.5°C. The parameters of the shape memory performance, recovery ratio (R_r) and fixity ratio (R_f), are defined as equations 2 and 3, respectively.

$$R_r = \frac{L_1 - L_3}{L_1}$$ Eq. 2,

$$R_f = \frac{L_2}{L_1}$$ Eq. 3;

L_1, L_2 and L_3 represent the stretched length at the elevated temperature, the length after unloading the applied force and the specimen length at the end of the recovery process.

2.7. Cell Culture Procedure

The Human Foreskin Fibroblast (HFF) cells were seeded onto the thermoset PU/CNW nanocomposites according to the procedure described in detail in our previous paper (Jafari et al., 2020). Here, we describe the procedure in summary: 1) washing the PU films with distilled water and after drying, they were UV-sterilized; 2) Tissue-culture grade polystyrene (TCPS, 48 wells) was used for cell seeding onto the tPU/CNW nanocomposite films; 3) HFF cells suspended in DMEM, with 10% FBS and 1% penicillin/ streptomycin, with a cell density of 2×10^4 cells/specimen were seeded on the tPUs; 4) Using the standard condition of 37°C with 96% humidity and 5% CO_2 atmosphere in the incubator for maintaining the seeded cells; 5) The cell fixing was performed by 2.5% glutaraldehyde. The cell viability of the HFF cells seeded onto the tPU/CNW nanocomposites was measured through MTT assay. After 3 and 5 days of culture, 50 ml of MTT solution (5 mg/ml) was added to each one of the wells. The plates then were incubated for three hours. At the end, the supernatant was collected and a micro-plate reader (BioTek) was used for analysis of optical density. The cell viability is measured using Eq. 4.

Cell Viability (%) = $\frac{OD}{OD_0} \times 100$ Eq. 4

OD and OD_0 represent the optical density of suspensions related to cell-seeded plates and the blank control, respectively.

2.6Characterization

The chemical structure analysis was performed using ATR-FTIR (MOD SRG 1100G, BOMEM) and Raman spectroscopy (Confocal Raman Microscope, equipped with two laser wavelengths of 532 and 785 nm). Scanning electron microscopy (SEM), Phenom Pharos, used for surface and cross-section imaging. Dynamic mechanical analysis (DMA, Triton, TA) was performed for phase behavior and shape memory performance analyses. Differential scanning calorimetry (DSC, Mettler/Toledo) was used for analysis of crystallization with a heating and cooling rate of 10 ℃/min. The stress-strain analysis was performed using the tensile instrument (BONGSHIN, model: DBBP-2 t) with a jaw speed of 20 mm/min. The surface topography of the thermoset PU/CNW nanocomposites was analyzed using AFM (NT-MDT co.) instrument operating at room temperature in tapping mode. Inverted fluorescent microscopy was used to analyze the state of the seeded HFF cells after three and five days. For this analysis, the cells were fixed and treated with DAPI for cell staining.

3. Results And Discussion

3.1. Structural Analysis

3.1.1. Raman Spectroscopy

Raman spectroscopy is considered as a powerful chemical and physical characterization technique to study the molecular features of materials including conformational isomerism, chemical nature and the changes in crystallization of the polymer segments. For polymers consisting of polarizable parts, their crystallization affects their conformational structure and Raman spectroscopy can be used quantitatively and the results are more valid than the infrared spectroscopy results (Parnell et al., 2003). According to Fig. 1a, the characteristic Raman bands of crystalline and amorphous PCL segments are summarized as follow: 917 cm^{-1} (ν -**C-C** (= O)-O-) crystalline, 1030–1120 cm^{-1} (skeletal stretching, 1071 cm^{-1} ν –**C-O-C**- crystalline), 1276–1352 cm^{-1} (ω CH_2), 1410–1487 cm^{-1} (δ CH_2, 1445 crystalline), 2835–3000 cm^{-1} (ν CH, crystalline); regarding PTMG, the Raman bands are as follow: 2939, 2887, 2840 cm^{-1} (alkyl chains), 1478, 1442 cm^{-1} (bending mode of C-H group), 1278, 1226 cm^{-1} (CH twisting vibrations), 1123–1146 cm^{-1} (C-O, C-OH, C-C), 846, 860 cm^{-1} (skeletal vibrations), and 533, 362 cm^{-1} C-O-C bending (Tian et al., 2019; H. Wu et al., 2021). The Raman spectrum of the blend, block copolymer and their mixture indicate presence of both PCL and PTMG segments.

Figure 1b shows the Raman spectrum of the synthesized thermoset PU/CNW nanocomposites. The characteristic isocyanate bands, which are -N = C = O asymmetric stretch at 2272 cm^{-1} and symmetric stretch at 1443 cm^{-1} are absent in the spectrum as an indication of complete consumption of the functionality. Based on the images, the polyurethane bands are as follows: -NH- (amide I 1732 cm^{-1}, amide II 1530 cm^{-1}, amide III 1303 cm^{-1}), Ester υ(C = O) (urethane amide I υ(C = O) 1732 cm^{-1}, $\delta(CH_2)$: 1443 cm^{-1} and δ(CH) (urethane amide III 1249) (Ha et al., 2019; Qu et al., 2021). The band related to the ester carbonyl group is not available in the Raman spectrum of the PTMG-tPU and its intensity for the other three tPU specimens is lower than that of PCL-tPU.

3.1.2. FTIR Analysis

Figure 1c represents the whole FTIR spectrum of the synthesized thermoset PU nanocomposites of PCL_{2000}, $PTMG_{2000}$ and their different configurational structures. The absorption peaks in the wavenumber range of 900–1800 cm^{-1}, which is represented in Fig. 1d, provides the structural information of the polyols and the urethane functionality. Based on Fig. 1c, the absorption peak around 3332 cm^{-1} corresponds to the stretching vibrations of –NH- groups in the urethane group formed by the condensation reaction between the –N = C = O group in the prepolymers' structure and the –CH2-OH groups available on the CNW surface. The –NH- group in the urethane group usually shows two absorption peaks at 3330 and 3340 cm^{-1}, which are related to hydrogen-bonded and free –NH- groups. The single absorption peak at around 3332 cm^{-1} is due to the lack of free –NH- vibrations. The double

peak available in the range of 2800–3000 cm^{-1} corresponds to the stretching vibrations of -CH- groups in the organic polymer structure. Absence of the peak at 2200 cm^{-1} for all the specimens indicates that the –N = C = O reaction conversion has been completed (Noormohammadi et al., 2021a). Regarding the highlighted region, Fig. 1d, the $PTMG_{20000}$ polyol is distinguished from PCL_{2000} and other polyols, which contain both PCL and PTMG segments, by the absence of the carbonyl (-C(= O)-) peak at 1734 cm^{-1} (Sarkhosh et al., 2021). The carbonyl peak in the range of 1700–1750 cm^{-1} is characteristic of crystalline or amorphous polyesters. Moving towards lower wavenumbers, the two peaks available at 1624 cm^{-1} and 1575 cm^{-1} correspond to the stretching vibrations of –C(= O)- and bending vibrations of –NH- functionalities in the urethane structure (-NH-C(= O)-), respectively (Jafari et al., 2020). The intense peak at 1105 cm^{-1} available for all the specimens corresponds to stretching vibrations of alkoxy group. The peak at 1170 cm^{-1}, which is present only for polyols with PCL segments, is specific of ester functionalities (Nourany et al., 2021).

3.2. Morphological Analysis

Figure 2 shows the SEM cross-sectional and surface images of PCL-tPU, Block 1:1-tPU and PTMG-tPU nanocomposites of CNW. The first and second row images show the cross-sectional images of the cryo-fractured specimens. Based on these images, the CNW nanoparticles with 1.0 wt% content are uniformly distributed and dispersed and there is not any sign of clustering even at 5 μm scale. The reason for absence of any CNW aggregation or clustering is the covalent attachment of the nanoparticles to the matrix chains (Jafari et al., 2020; Noormohammadi et al., 2021a). The third row shows the SEM surface images of the specimens with 1 μm scale. The images show that the CNWs are aligned on the surface, parallel to the normal line of the cross-sectional surface, and they seem to have integrated to the matrix.

3.3. DMTA Analysis

The viscoelastic properties of thermoset PUs can be evaluated by DMTA instrument. The results of this test provides insights into the changes in the microstructure of the specimens and the results consist of storage (E') and loss (E") modulus. The ratio of E" and E' is called tanδ, which is used to identify the second order transitions (Nourany et al., 2021). In a common logE' vs. temperature, there are three main regions and two transitions. The regions are glassy, rubbery plateau and melt states. The two main transitions are glass transition temperature (T_g) and flow (or melting) temperature, which are second and first order transitions, respectively (Sarkhosh et al., 2021). For thermoset polymers, the flow of the specimens are absent and for a semi-crystalline polyol, the melting process of the crystallites can be identified as a one-order of magnitude fall in the storage modulus (Ranjbar et al., 2021). The PUs with linear morphology, also called thermoplastic polyurethanes (TPUs), show another second order transition for the hard segments in a higher temperature range compared to the soft segments (Jafari et al., 2020). Based on Fig. 3a, it can be seen that the transition for the hard segments is absent as they are immobilized through covalent bonding to the CNWs and cannot go through a long-range segmental movement. Lack of an upturn in tanδ curves in the temperature range of 50 to 80°C, Fig. 3b, confirms

absence of this transition (Noormohammadi et al., 2021a). As it can be seen from Fig. 3a, the T_g transition of the soft domain segments of all the specimens are very broad and extends from − 85°C to + 15°C. This feature is specific of semi-crystalline soft segments while amorphous soft segments show an abrupt fall in this region. This feature has also manifested itself in the wide temperature range of tanδ peak for this transition. Amorphous soft segments usually have a tanδ peak height of about 0.5 or higher with a relatively narrow width (Jafari et al., 2020). However, the specimens possess a very low peak height (below 0.14) confirming their semi-crystalline nature. The tanδ peak heights of each PU specimen is shown in Fig. 3c alongside their T_g.

Regarding the storage modulus (E') of the specimens, which is critical in determining the shape memory parameters, it remains high and constant at elevated temperatures. This is due to the thermoset nature of the PU nanocomposites. A high E', well above 10 MPa even at 100°C, creates a large driving force for shape recovery process (K. Zhang et al., 2019). Another distinct feature of the PU/CNW thermosets is the strong temperature dependency of E' in the temperature range of -85 to + 15°C, which acts as a tool for tuning the shape fixity of the specimens (Argun et al., 2019; Kolesov et al., 2015; Zeng et al., 2021).

The soft domain T_g transition of each specimen is also shown in Fig. 3c. The interesting phenomenon that has occurred is that the T_g values of the thermoset PU specimens composed of both PCL and PTMG segments are lower than the T_g values of the soft segments composed of only PCL_{2000} or $PTMG_{2000}$. They have also shown higher tanδ peak height. Neat PCL's T_g is around − 61 ± 1 °C, while for PTMG the T_g value is -65°C (Bershtein et al., 2005; Zhuravlev et al., 2011).

Compared to PCL_{2000} and $PTMG_{2000}$ segments, both polymers have experienced an increase of about + 14°C in their T_gs once they are used in the thermoset PU/CNW structure. Chemical confinement of the polyols restricts the soft segments' motion and reducing the ease of soft segment rotation. The declined segmental motion of the PCL_{2000} and $PTMG_{2000}$ segments in the PCL-tPU and PTMG-tPU specimens is responsible for the + 14°C increase in their T_g. The interesting fact is that both the PCL_{2000} and $PTMG_{2000}$ soft segments have experienced almost the same extent of increase. The negligible variation can be due to the small difference in their chain flexibility as indicated by the 4 degree difference in their T_g. The reason behind the lower values of T_gs for soft domain chains with different combinations of PCL and PTMG segments can be explained by their increased chain dynamics (Jafari et al., 2020). The lower T_g values indicate higher segmental mobility as it manifests itself in the slight increase in tanδ peak heights related to the specimens. The lowest T_g value corresponds to the Blend-tPU specimen, with soft domains composed of PCL_{2000} and $PTMG_{2000}$, and the highest tanδ peak height is also corresponds to this specimen. The soft domain of the Blend-tPU specimen is composed of incompatible segments and the single tanδ peak behavior of the soft domain indicates their increased miscibility. The increase in phase miscibility of two semi-crystalline polymers results in a decrease in order and consequently a decline in their crystallization ability. The same concept is applicable for Block 1:1-tPU and mixture-tPU specimens. The impact of morphological and compositional complexity on crystallization potential of the soft domain chains will be discussed later in the DSC and XRD results.

3.4. Soft Domain Crystallization

3.4.1. DSC Analysis

For a system of two incompatible semi-crystalline segments, the characteristic crystallization parameters provide insights into the phase organization of the segments. Based on Fig. 4a and b, and the information summarized in Table 2, the PCL_{2000} has the highest crystallization (T_c) and melting (T_m) temperatures of 26.6 and 51.7℃. $PTMG_{2000}$ has a T_c and T_m of 12.8 and 25.7℃. Block copolymerization of these two polymers with PCL_{1000}-$PTMG_{2000}$-PCL_{1000} ABA architecture has led to two distinct crystallization peaks at 18.5, 8.3℃ and three melting peaks at 39.3, 33.7, and 22.8℃. Besides the depression of crystallization and melting peak points for both polymer segments, the crystallization enthalpies has also experienced a decline compared to neat PCL_{2000} and $PTMG_{2000}$. Regarding the T_cs, the peak points of + 18.5 and + 8.3℃ correspond to PCL_{1000} and $PTMG_{2000}$blocks, respectively. As a general fact, block copolymerization of two semi-crystalline polymers reduces their thermal stability through changing their crystallites' morphology, which is dependent on their block lengths (Müller et al., 2002; Nojima et al., 1995). The melting temperatures of 39.3 and 33.7℃ correspond to PCL segments and the peak at 22.8℃ is related to the $PTMG_{2000}$ block. The PCL crystallites have a higher thermal stability compared to the PTMG crystallites as it can be inferred from the higher T_c and T_m of PCL polyol. Therefore, initially the PCL segments would undergo crystallization, as their nucleation starts at higher temperatures, leading to the partial freezing of the block copolymer system. Early crystallization of PCL segments would affect the PTMG crystallization and increase the imperfectness of its crystallites. The covalent attachments of the PCL_{1000} and $PTMG_{2000}$ blocks in an ABA architecture limits their phase separation and increases disorder in the block copolymer chain. These structural features affect the crystallites' morphology and thermal stability of both crystallizable blocks.

The depression in the characteristic temperatures are lesser in the Blend sample. The PCL_{2000} and $PTMG_{2000}$ chains are not covalently connected to each other and upon cooling they can easily segregate and form relatively stable crystallites and the characteristic crystallization would not be impacted greatly. The reason for the decline in the characteristic temperatures is a combination of kinetics and thermodynamics effects. The kinetics works in the course of crystallization and impacts the lamella thickness (L), which is related to T_m through Eq. 5. This equation indicates that the lower L results in lower T_m (Castillo & Müller, 2009; He & Xu, 2012).

$$T_m = T_m^0 . \left(1 - \frac{2v_e}{\Delta H_f L}\right) \text{ Eq. 5,}$$

Here, v_e is the free energy of chain folding at the lamella's surface and $\Delta H_f$is the lamella heat fusion. As mentioned earlier, covalent attachment of the two incompatible polymers limits their phase separation and this structural feature affects the crystallites' morphology and predominantly reduces L and a reduction in T_m of each block would be a direct result of this change (H.-L. Chen et al., 2001).

From thermodynamic point of view, the controlling parameter of the changes in thermal stability of the crystallites is the product of the interaction parameter (χ_{AB}) and the block lengths (N), i.e. χ_{AB}.N. For higher block lengths the impact of covalent bonding on the characteristic temperatures would be lower (Vilgis & Halperin, 1991).

Table 2
The crystallization and melting temperatures of the polyols and the soft segments in the thermoset PU structure.

Sample	Tc (°C)	Tm (°C)	Sample	Tc (°C)	Tm (°C)
PCL_{2000}	26.6	51.7	**PCL-tPU**	-18.0	3.1
$PTMG_{2000}$	12.8	25.7	**PTMG-tPU**	-25.0	4.1
Block 1:1	18.5, 8.3	39.3, 33.7, 22.8	**Block 1:1-tPU**	-29.5	-5.9
Blend	25.0, 10.8	45.7, 43.3, 25.0	**Blend-tPU**	-33.0	-4.4
mixture	21.6, 7.9	47.4, 34.5, 22.0	**mixture-tPU**	-32.0	-2.4

For the mixture specimen, the depression in T_c and T_m of PCL segments are not very large compared to the Block 1:1 specimen. The reason for the relatively higher T_c and T_m of PCL segments can be defined as follows: higher crystallization temperature of PCL segments compared to PTMG segments results in their early crystallization, which results in crystallization-assisted phase separation of PCL segments. Presence of the block copolymer reduces the interfacial tension between the incompatible PCL and PTMG domains, hence, reducing the extent of phase separation and resulting in smaller domains of PCL and PTMG (He & Xu, 2012; Müller et al., 2002).

Regarding the thermoset PU-CNW specimens, as their crystallization and melting spectrum are represented in Fig. 4c and d, the polyols as soft segments have experienced an enormous decline in their crystallization potential. As a general fact, incorporation of semi-crystalline polyols into polyurethane structure leads to a decline in their crystallization ability, however, as reported in our previous paper (Jafari et al., 2020), thermoset PUs of PEG-PCL polyols with CNWs had a larger impact compared to their thermoplastic counterparts. The reasons behind these sharp declines are: 1) chemical attachment of the polyol chains to CNWs, which highly limits their kinetics of crystallization, and 2) the repulsive interaction between the polyols and the urethane functionalities (Khadivi et al., 2019; Saralegi et al., 2013; Shirole et al., 2018). According to the summarized data in Table 2, the Blend-tPU, Block 1:1-tPU and mixture-tPU specimens have negative T_m values and their T_c values are the lowest compared to tPUs of PCL_{2000} and $PTMG_{2000}$. This result is in accordance with the results shown for the polyols as block copolymerization and blending reduces the thermal stability of the crystallites. Therefore, the adverse impact of thermosetting on these soft segments would be higher.

3.4.2. X-Ray Diffraction Analysis

The XRD analysis provides information on the structure of the crystallites' unit cells and the impact of crystallites' perfection or defects can be seen as the changes in their 2θ positions, the width and the intensity of the peaks. Based on Bragg's law, Eq. 6, the change in 2θ positions directly changes the d-spacing (Nourany et al., 2021), (Noormohammadi et al., 2021a).

$n\lambda = 2dsin(\theta)$ Eq. 6,

According to Fig. 4e, the PCL_{2000} polyol showed diffraction peaks at 2θ = 21.65, 22.22, and 23.95 °, which are attributed to the 110, 111 and 200 planes (Hoidy et al., 2010). $PTMG_{2000}$ showed two diffraction peaks at 2θ = 20.10 and 24.52 ° corresponding to d-spacing of 0.42 and 0.38 nm. According to the literature, block copolymerization of semi-crystalline polymers reduces their crystallization amount and as a direct result T_c and T_m decreases, which is an indication of lowered thermal stability of the crystallites. For the PCL_{1000}-$PTMG_{2000}$-PCL_{1000} block copolymer with hydroxyl end-groups (Block 1:1), the intensity of the diffraction peaks related to the PCL_{1000} blocks (2θ = 21.40, 22.03 and 23.73 °) have declined by about half and the peaks related to PTMG2000 have almost disappeared except for the peak available at 2θ = 20.18 °, with extremely low intensity. The results indicate that the block copolymerization had a higher impact on the middle block ($PTMG_{2000}$). The reason behind this result can be the higher T_g of PTMG compared to PCL and consequently lower chain dynamics, which affects its crystallization kinetics. The changes in 2θ degrees show the structural changes of crystallites' unit cells as the blocks are covalently attached and affect the nature of the morphology of the crystallites and their development (Jiang et al., 2001), (Luyt & Gasmi, 2016).

For the Blend polyol (1:1 w:w PCL_{2000}/$PTMG_{2000}$ blend), the peak positions have not experienced any significant change and only the diffraction peaks' intensities have declined. This is due to the fact that the two incompatible semi-crystalline polymers have not affected the crystallization thermodynamics and only crystallization kinetics has been impacted (Luyt & Gasmi, 2016). Compared to the homopolymers, for the mixture (the relative 1:1:1 weight ratios of $PTMG_{2000}$, PCL_{2000} and the block copolymer), the diffraction peak positions have shifted towards lower diffraction peaks (2θ= 21.46, 22.10, and 23.73 with a broad peaks at 20.18 °). Addition of the block copolymer into the blend reduces the interfacial tension between the two phases. This change improves the phase miscibility of the PCL and PTMG segments at the interface and limiting the extent of phase separation.

For the thermoset PU/CNW nanocomposites, as seen in the DSC results, the crystallization ability and the thermal stability of the crystallites reduces to a large degree. Based on Fig. 4f, the overall shape of the spectrums are broad indicating the amorphous nature of the polyol. Presence of a distinguishable peak at 2θ of 23.4 ° is related to the characteristic diffraction peak of CNW (Noormohammadi et al., 2021a). The 1.0 wt% content of the CNW allows for detection of their crystallites' structure.

3.5. Mechanical Properties

Since the thermoset PU/CNW nanocomposites do not contain any stable crystallite structures of soft segments at room temperature, they can be considered as rubbers and their deformation under a uniaxial stretching should follow the thermodynamics of rubbers (Vorov et al., 2008).

$$f = \left(\frac{\partial U}{\partial L}\right)_{T,V} + T\left(\frac{\partial f}{\partial T}\right)_{V,L} = f_E + f_S \quad \text{Eq. 7,}$$

Based on Eq. 7, the force f applied to the thermoset PU nanocomposites comprises of two factors, energetic and entropic contributions. Since the nanocomposites have amorphous state at room temperature, $f_E \cong 0$ and the entropic contribution is more dominant. The energetic contribution is more dominant in highly crystalline specimens in which stretching distorts the lattice spacing. At constant temperature, upon stretching the specimens, the soft segments face a decline in their conformational entropy and according to Eq. 8, the required force for further stretching increases (Stribeck et al., 2015).

$$f_S = T\left(\frac{\partial f}{\partial T}\right)_{V,L} = -T\left(\frac{\partial S}{\partial L}\right)_{T,V} \quad \text{Eq. 8,}$$

Overall, at low strains, λ < 1, the energetic contribution is negligible and the entropic contribution dominates. Based on Fig. 5a, upon stretching the specimens the stress required increases. According to Fig. 5a and Table 3, PCL-tPU had the highest elongation at break (ϵ_{u}, ultimate strain) of 289.0% and ultimate stress (σ_{u}) of 11.67 MPa, while PTMG-tPU had an ϵ_{u} and σ_{u} of 140.4% and 9.27 MPa, respectively. The ϵ_{u} of the block 1:1-tPU declines sharply with a value of 66.2% despite of having a higher soft segment length or higher molecular length between cross-link points (Mc). The Blend-tPU and mixture-tPU specimens have also experienced an intense decline in their ϵ_{u} and besides this change, their σ_{u} have also declined with a σ_{u} of 4.85 MPa for the Blend-tPU. Regarding the Young's modulus (E), as summarized in Table 3, Block 1:1-tPU specimen has the highest E value of 166.9 MPa. The E values are measured from the low-strain linear elastic regions of the stress-strain curves (Fig. 5b, below 2% strain). For a uniaxial deformation of a cross-linked system with the assumption of $\Delta V \cong 0$, no change in volume upon stretching, we have Eq. 9:

$$G = \frac{nkT}{V} = \nu kT = \frac{\rho RT}{M_s} \quad \text{Eq. 9,}$$

Based on this general equation for a network of a homopolymer, the modulus of the specimen increases as a linear function of number density of the strands (an increase in strand length decreases the number of strands per unit volume) (Scetta et al., 2021; Vorov et al., 2008). However, by looking at cross-link density (CLD, ν) of the specimens summarized in Table 3, it can be seen that the Block 1:1-tPU has the lowest CLD value. As the chemistry and configuration of soft domain chains differ, the Eq. 8 that has been developed for simple networks in uniaxial deformations fails to predict the overall trend of the mechanical behavior.

One possible explanation for the peculiar behavior can be found in the elastic modulus of the specimens at room temperature. According to Fig. 4a, the E' of PTMG-tPU and mixture-tPU are around 30 and 60 MPa, respectively. However, the E' values of the remaining specimens are in the range of 100–200 MPa, which are roughly in correlation with the Young's modulus of the specimens. The rod-like morphology of the highly crystalline CNW and its chemical bonding to the prepolymer chains would have also played a key role in controlling the mechanical properties of the thermoset PU/CNW nanocomposites.

Table 3
The characteristic mechanical properties of the thermoset PU/CNW nanocomposites.

Specimen	ϵ_u (%)	σ_u (MPa)	E (MPa)	$\upsilon \times 10^7$ (mol/cm^3)
PCL-tPU	289.0 ± 7.1	11.67 ± 0.39	100.1 ± 3.6	23.9 ± 1.3
PTMG-tPU	140.4 ± 5.6	9.27 ± 0.17	40.7 ± 2.1	24.2 ± 0.5
Block 1:1-tPU	66.2 ± 3.9	9.48 ± 0.13	166.9 ± 5.8	13.7 ± 0.8
Blend-tPU	116.5 ± 4.2	4.85 ± 0.15	56.4 ± 3.7	22.8 ± 1.1
Mixture-tPU	121.4 ± 5.0	7.66 ± 0.21	73.9 ± 2.9	19.4 ± 0.9

The Young's modulus of the thermoplastic PUs, depending on the curing process and the nature of the Diisocyanate, is usually below 10 MPa (Tito et al., 2019; Xiang et al., 2021). The high E values of the thermoset PU/CNW nanocomposites suggests that the CNWs, as high modulus rod-like nanoparticles, have played a key role in increasing the strength and elasticity of the thermoset PUs. As shown in SEM images, the CNWs are dispersed in the matrix in a relatively uniform way, which is due to the fact that the chemical bonding of the nanoparticles to the prepolymer prohibits their self-assembly and further clustering.

3.6. Shape Memory Performance

According to Fig. 5c, the digital photographs of the PCL-tPU and mixture-tPU specimens, in a room-temperature recovery process, show that the specimens have a high shape recovery ability. In a more systematic study, the glass transition phenomena, as a dynamic process with a relatively wide transition temperature range, is usually considered as the base for selection of the fixity temperature (Garle et al., 2012; Zeng et al., 2021). In this research, the three different temperatures of -50, -25 and 0°C were selected for evaluation of the fixity ratio (R_f) of each specimen. Figure 5d shows the change in R_f as a function of temperature for each specimen. The results indicate that as the temperature increases, the ability of the specimens to fix their temporary shape declines. The reason for this change is the gradual decline of elastic modulus after the T_g transition and an increase in soft segment entropy, which tends to regain the relaxed state (W. Du et al., 2021; Gao et al., 2018; Nessi et al., 2019; Zare et al., 2019). For amorphous polymers, the decline in elastic modulus after T_g is sharp and the temperature dependency of R_f is not very strong. However, for the tPUs with semi-crystalline nature, the temperature dependency of R_f

is strong (Gupta & Mekonnen, 2022; K. Zhang et al., 2019). Based on the results, the highest shape fixity of 100% corresponds to PCL-tPU at -50°C, which is due to the fact that this temperature is below its T_g and the soft segments lack any elastic recovery (S. Chen et al., 2010; X. L. Wu et al., 2014; Yu et al., 2014). According to the literature, elastic modulus is responsible for controlling shape fixity and crystallization of the soft segments, as a key factor, also increase the elasticity of the specimens in the plateau region (Argun et al., 2019; Kumar Patel & Purohit, 2018). At the temperature of -25°C, the R_f is still high for all the specimens, which is due to the fact that melting temperatures of the existing crystallites are well above this temperature. The temperature of 0°C is very close to T_m of the crystallites, slightly below or above T_m for each specimen, which in turn cause a sharp decline in R_f, as presented in Fig. 5d. Figure 5e shows the DMA results of the shape memory performance analysis for the shape fixity temperature of -25°C and the recovery temperature of + 37.5°C. According to the DMTA results, the specimens possessed a high elastic modulus (above 30 MPa) even at higher temperatures, which is due to the thermoset nature of the specimens and the presence of the high modulus CNW nanoparticles. Based on Table 4 and Fig. 5e, except for the PTMG-tPU and mixture-tPU specimens, the remaining three specimens showed a very high recovery ratios, falling in the range of 95–98%. The reason for the high R_r of the three specimens can be their high and stable elastic modulus compared to the other two specimens. The advantage of thermoset PUs over thermoplastic PUs is their constant elastic modulus at elevated temperatures and over a wide temperature range, which is a sign of a constant entropic driving force for recovering the original shape (Sarkhosh et al., 2021).

Table 4
The shape memory parameters of the synthesized thermoset PU nanocomposites fixed at -25°C with recovery temperature of + 37.5°C.

Specimen	Fixity ratio (%)	Recovery ratio (%)	X-link degree (%)
PCL- tPU	94	98	97 ± 1
PTMG- tPU	90	86	98 ± 1
Block 1:1- tPU	93	95	96 ± 2
Blend- tPU	92	96	97 ± 1
Mixture- tPU	88	89	98 ± 2

In a PU structure, the soft domain is the active phase for recovering the original shape and upon stretching the specimens at elevated temperatures, the chains in the active phase experience a decline in their conformational entropy (Jiu et al., 2016; Y. Zhang et al., 2019). By keeping the applied force and decreasing temperature, parts of the stretched chain segments are aligned in the crystalline structures (Barot et al., 2008; Bouaziz et al., 2017). Upon removing the force at -25°C, since the temperature is well above T_g transition, the specimens experience a partial spontaneous shape recovery. However, as the temperature increases, the segments tend to increase their conformational entropy and shrink in size (K. Zhang et al., 2019; Zhou et al., 2014), which in our case it is expressed as a decrease in longitudinal

length. For a thermoset system, the most important parameter in determining the shape recovery ratio is the cross-link degree, which provides a network point for reducing the chain slippage and energy dissipation ability of the soft segments (Gao et al., 2018; Li et al., 2018). In reality, achieving an ideal chemical network is practically impossible. However, the CNWs with abundant hydroxyl groups were able to create a high cross-linking degree being in the range of 96–98%. The reason for the high and close to each other can be the abundance of hydroxyl groups, which serve as the cross-linking point for the prepolymers (Nourany et al., 2021; Ranjbar et al., 2021). Since the cross-linking degrees of the thermoset PUs were high and close to each other, the elastic modulus was considered to be the main parameter in determining the final shape recovery at the experimental time period.

3.7. Cell Culture Analysis

MTT assay is performed on the specimens using HFF cells to evaluate their cytotoxicity. The viability of the cells on the specimens relative to the control TCPS culture plate is considered as a basis for evaluating the cytotoxicity of the specimens (Nourany et al., 2021). Based on the statistical results of the MTT assay presented in Fig. 6 (top image), in the first three days of the culturing, the cell growth on the specimens compared to the control is low being around 76%. The lowest cell growth is for Block 1:1-tPU with a relative cell growth of 68%. After 5 days of cell culture, the seeded HFF cells tend to grow with an average relative cell growth of 102%.

The lowest cell growth was again corresponded to the Block 1:1-tPU specimen with a relative cell growth of 93%. The reason for the lower relative cell growth can be the induction time for cell attachment (Ranjbar et al., 2021). The reason for the low cell viability of the Block 1:1-tPU can be the presence of free CNWs as this specimen has the lowest cross-link density. Overall, cell viability of 90% or higher for the materials is considered to be non-toxic and based on the results of 5 days, the specimens are considered to be highly biocompatible (Nourany et al., 2021). The fluorescent images of PCL-tPU, Block 1:1-tPU and PTMG-tPU shown in Fig. 6 indicate that the cell density and growth is higher for PCL-tPU and PTMG-tPU. Based on the images, the cell density of the Block 1:1-tPU is lower compared to the other thermoset PU/CNW nanocomposites.

4. Conclusion

The results of shape memory analysis indicated that the thermoset PUs of the semi-crystalline polyols possessed high shape recovery with R_r values in the range of 86–98%. There was a direct correlation between the storage modulus (E') and R_r values as the thermoset PU/CNW nanocomposites showed stable and high E' at temperatures above 20°C. This is mainly due to their thermoset nature and presence of CNWs with high elastic modulus. The tanδ peak height of the specimens was below 0.14, which is specific of highly elastic specimens. The results of shape fixity analysis at the three different temperatures of -50, -25 and 0°C indicate the specimens have higher shape fixity at temperatures close to T_g transition. The wide T_g transition provided the ability to tune the shape fixity ratio of the specimens and the highly elastic nature of the tPUs resulted in high R_r and R_f values. The SEM and 3D AFM

topographical images showed that the CNWs with rod-like morphology have not formed any visible clusters, which was attributed to the chemical bonding of the CNWs to the prepolymers. Despite the adverse impact of the sharp decline of soft segments' crystallization on elastic modulus, the uniform distribution of CNWs with 1.0 wt% content has led to low. The low tanδ height values is an indication of highly elastic modulus. The specimens showed to be highly biocompatible and HFF cell showed high cell adhesion and growth after 5 days of cell culture.

Declarations

Acknowledgement: This work was partially funded by Amirkabir University of Technology.

Conflict of Interest: The authors have no conflict of interest.

Data Availability: The experimental data will be provided by the corresponding author upon reasonable request.

Credit of Authorship: Elahe Aboueimehrizi: Data acquisition, data validation, formal analysis, writing the original draft; Mohammad Amin Makaremy, Sina Bazrpash, Fatemeh Noormohammadi: Data validation, formal analysis, editing the original draft; Yasaman Rahimi Darestani: Data acquisition, formal analysis; Mohammad Nourany: Conceptualization, data validation, writing the original draft, funding and grant acquisition.

References

1. Argun A, Gulyuz U, Okay O (2019) Semi-Crystalline, Three-Segmented Hybrid Gels with Multiple Shape-Memory Effect. Macromolecular Symposia 385(1):1800164. https://doi.org/https://doi.org/10.1002/masy.201800164
2. Barot G, Rao IJ, Rajagopal KR (2008) A thermodynamic framework for the modeling of crystallizable shape memory polymers. Int J Eng Sci 46(4):325–351. https://doi.org/https://doi.org/10.1016/j.ijengsci.2007.11.008
3. Bershtein VA, David L, Egorov VM, Fainleib AM, Grigorieva O, Bey I, Yakushev PN (2005) Structural/compositional nanoheterogeneity and glass-transition plurality in amorphous polycyanurate–poly(tetramethylene glycol) hybrid networks. J Polym Sci Part B: Polym Phys 43(22):3261–3272. https://doi.org/https://doi.org/10.1002/polb.20614
4. Bouaziz R, Roger F, Prashantha K (2017) Thermo-mechanical modeling of semi-crystalline thermoplastic shape memory polymer under large strain. Smart Mater Struct 26(5):55009. https://doi.org/10.1088/1361-665x/aa6690
5. Cao F, Jana SC (2007) Nanoclay-tethered shape memory polyurethane nanocomposites. Polymer 48(13):3790–3800. https://doi.org/https://doi.org/10.1016/j.polymer.2007.04.027
6. Castillo RV, Müller AJ (2009) Crystallization and morphology of biodegradable or biostable single and double crystalline block copolymers. Prog Polym Sci 34(6):516–560.

https://doi.org/https://doi.org/10.1016/j.progpolymsci.2009.03.002

7. Chen H-L, Hsiao S-C, Lin T-L, Yamauchi K, Hasegawa H, Hashimoto T (2001) Microdomain-Tailored Crystallization Kinetics of Block Copolymers. Macromolecules 34(4):671–674. https://doi.org/10.1021/ma001485e
8. Chen S, Hu J, Zhuo H, Yuen C, Chan L (2010) Study on the thermal-induced shape memory effect of pyridine containing supramolecular polyurethane. Polymer 51(1):240–248. https://doi.org/https://doi.org/10.1016/j.polymer.2009.11.034
9. Choi JT, Dao TD, Oh KM, Lee H, Jeong HM, Kim BK (2012) Shape memory polyurethane nanocomposites with functionalized graphene. Smart Mater Struct 21(7):75017. https://doi.org/10.1088/0964-1726/21/7/075017
10. Domingues RMA, Gomes ME, Reis RL (2014) The Potential of Cellulose Nanocrystals in Tissue Engineering Strategies. Biomacromolecules 15(7):2327–2346. https://doi.org/10.1021/bm500524s
11. Du H, Liu W, Zhang M, Si C, Zhang X, Li B (2019) Cellulose nanocrystals and cellulose nanofibrils based hydrogels for biomedical applications. Carbohydr Polym 209:130–144. https://doi.org/https://doi.org/10.1016/j.carbpol.2019.01.020
12. Du W, Zhang Z, Yin C, Ge X, Shi L (2021) Preparation of shape memory polyurethane/modified cellulose nanocrystals composites with balanced comprehensive performances. Polym Adv Technol 32(12):4710–4720. https://doi.org/https://doi.org/10.1002/pat.5464
13. Fortunati E, Luzi F, Janke A, Häußler L, Pionteck J, Kenny JM, Torre L (2017) Reinforcement effect of cellulose nanocrystals in thermoplastic polyurethane matrices characterized by different soft/hard segment ratio. Polym Eng Sci 57(6):521–530. https://doi.org/https://doi.org/10.1002/pen.24532
14. Gao Y, Liu W, Zhu S (2018) Reversible Shape Memory Polymer from Semicrystalline Poly(ethylene-co-vinyl acetate) with Dynamic Covalent Polymer Networks. Macromolecules 51(21):8956–8963. https://doi.org/10.1021/acs.macromol.8b01724
15. Garle A, Kong S, Ojha U, Budhlall BM (2012) Thermoresponsive Semicrystalline Poly(ε-caprolactone) Networks: Exploiting Cross-Linking with Cinnamoyl Moieties to Design Polymers with Tunable Shape Memory. ACS Appl Mater Interfaces 4:645
16. George J, Sabapathi SN (2015) Cellulose nanocrystals: synthesis, functional properties, and applications. Nanatechnol Sci Appl 8:45–54. https://doi.org/10.2147/NSA.S64386
17. Gupta A, Mekonnen TH (2022) Cellulose nanocrystals enabled sustainable polycaprolactone based shape memory polyurethane bionanocomposites. J Colloid Interface Sci 611:726–738. https://doi.org/https://doi.org/10.1016/j.jcis.2021.11.174
18. Ha Y, Kim Y-O, Ahn S, Lee S, Lee J, Park M, Chung JW, Jung YC (2019) Robust and stretchable self-healing polyurethane based on polycarbonate diol with different soft-segment molecular weight for flexible devices. Eur Polymer J 118:36–44. https://doi.org/https://doi.org/10.1016/j.eurpolymj.2019.05.031
19. He W-N, Xu J-T (2012) Crystallization assisted self-assembly of semicrystalline block copolymers. Prog Polym Sci 37(10):1350–1400.

https://doi.org/https://doi.org/10.1016/j.progpolymsci.2012.05.002

20. Hoidy WH, Al-Mulla EAJ, Al-Janabi KW (2010) Mechanical and Thermal Properties of PLLA/PCL Modified Clay Nanocomposites. J Polym Environ 18(4):608–616. https://doi.org/10.1007/s10924-010-0240-x
21. Jafari S, Nourany M, Zakizadeh M, Taghilou A, Ranjbar HA, Noormohammadi F (2020) The effect of controlled phase separation of PEG/PCL-2000 homopolymer polyols using their PCL500-PEG1000-PCL500 tri-block copolymer and CNCs in the final polyurethane hydrogels on their shape memory behavior. Compos Commun 19:194–202. https://doi.org/10.1016/j.coco.2020.03.016
22. Jiang S, Ji X, An L, Jiang B (2001) Crystallization behavior of PCL in hybrid confined environment. Polymer 42(8):3901–3907. https://doi.org/https://doi.org/10.1016/S0032-3861(00)00565-6
23. Jiu H, Jiao H, Zhang L, Zhang S, Zhao Y (2016) Graphene-crosslinked two-way reversible shape memory polyurethane nanocomposites with enhanced mechanical and electrical properties. J Mater Sci: Mater Electron 27(10):10720–10728. https://doi.org/10.1007/s10854-016-5173-2
24. Joo Y-S, Cha J-R, Gong M-S (2018) Biodegradable shape-memory polymers using polycaprolactone and isosorbide based polyurethane blends. Mater Sci Engineering: C 91:426–435. https://doi.org/https://doi.org/10.1016/j.msec.2018.05.063
25. Kausar A (2019) Shape memory polyurethane/graphene nanocomposites: Structures, properties, and applications. J Plast Film Sheeting 36(2):151–166. https://doi.org/10.1177/8756087919865296
26. Khadivi P, Salami-Kalajahi M, Roghani-Mamaqani H, Lotfi M, Sofla R (2019) Fabrication of microphase-separated polyurethane/cellulose nanocrystal nanocomposites with irregular mechanical and shape memory properties. Appl Phys A 125(11):779. https://doi.org/10.1007/s00339-019-3082-y
27. Kolesov I, Dolynchuk O, Radusch HJ (2015) Shape-memory behavior of cross-linked semi-crystalline polymers and their blends. Express Polym Lett 9(3):255–276. https://doi.org/10.3144/expresspolymlett.2015.24
28. Kumar Patel K, Purohit R (2018) Future Prospects of shape memory polymer nano-composite and epoxy based shape memory polymer- A review. *Materials Today: Proceedings*, *5*(9, Part 3), 20193–20200. https://doi.org/https://doi.org/10.1016/j.matpr.2018.06.389
29. Kumar TP, Saravanakumar S, Sankaranarayanan K (2011) Effect of annealing on the surface and band gap alignment of CdZnS thin films. Appl Surf Sci 257(6):1923–1927. https://doi.org/https://doi.org/10.1016/j.apsusc.2010.09.027
30. Lahiji RR, Xu X, Reifenberger R, Raman A, Rudie A, Moon RJ (2010) Atomic Force Microscopy Characterization of Cellulose Nanocrystals. Langmuir 26(6):4480–4488. https://doi.org/10.1021/la903111j
31. Landa M, Canales J, Fernández M, Muñoz ME, Santamaría A (2014) Effect of MWCNTs and graphene on the crystallization of polyurethane based nanocomposites, analyzed via calorimetry, rheology and AFM microscopy. Polym Test 35:101–108. https://doi.org/https://doi.org/10.1016/j.polymertesting.2014.03.008

32. Li M, Guan Q, Dingemans TJ (2018) High-Temperature Shape Memory Behavior of Semicrystalline Polyamide Thermosets. ACS Appl Mater Interfaces 10(22):19106–19115. https://doi.org/10.1021/acsami.8b03658
33. Liu Y, Li Y, Yang G, Zheng X, Zhou S (2015) *Multi-Stimulus-Responsive Shape-Memory Polymer Nanocomposite Network Cross-Linked by Cellulose Nanocrystals*. *Mdi*. https://doi.org/10.1021/am5081056
34. Lu P, Hsieh Y-L (2010) Preparation and properties of cellulose nanocrystals: Rods, spheres, and network. Carbohydr Polym 82(2):329–336. https://doi.org/https://doi.org/10.1016/j.carbpol.2010.04.073
35. Luyt AS, Gasmi S (2016) Influence of blending and blend morphology on the thermal properties and crystallization behaviour of PLA and PCL in PLA/PCL blends. J Mater Sci 51(9):4670–4681. https://doi.org/10.1007/s10853-016-9784-z
36. Mariano M, El Kissi N, Dufresne A (2014) Cellulose nanocrystals and related nanocomposites: Review of some properties and challenges. J Polym Sci Part B: Polym Phys 52(12):791–806. https://doi.org/10.1002/polb.23490
37. Mi H-Y, Jing X, Yilmaz G, Hagerty BS, Enriquez E, Turng L-S (2018) In situ synthesis of polyurethane scaffolds with tunable properties by controlled crosslinking of tri-block copolymer and polycaprolactone triol for tissue regeneration. Chem Eng J 348:786–798. https://doi.org/https://doi.org/10.1016/j.cej.2018.04.198
38. Mu R, Hong X, Ni Y, Li Y, Pang J, Wang Q, Xiao J, Zheng Y (2019) Recent trends and applications of cellulose nanocrystals in food industry. Trends Food Sci Technol 93:136–144. https://doi.org/https://doi.org/10.1016/j.tifs.2019.09.013
39. Müller AJ, Balsamo V, Arnal ML, Jakob T, Schmalz H, Abetz V (2002) Homogeneous Nucleation and Fractionated Crystallization in Block Copolymers. Macromolecules 35(8):3048–3058. https://doi.org/10.1021/ma012026w
40. Nessi V, Falourd X, Maigret J-E, Cahier K, D'Orlando A, Descamps N, Gaucher V, Chevigny C, Lourdin D (2019) Cellulose nanocrystals-starch nanocomposites produced by extrusion: Structure and behavior in physiological conditions. Carbohydr Polym 225:115123. https://doi.org/https://doi.org/10.1016/j.carbpol.2019.115123
41. Nojima S, Yamamoto S, Ashida T (1995) Crystallization of Block Copolymers IV. Molecular Weight Dependence of the Morphology Formed in ε-Caprolactone–Butadiene Diblock Copolymers. Polym J 27(7):673–682. https://doi.org/10.1295/polymj.27.673
42. Noormohammadi F, Nourany M, Mir Mohamad Sadeghi G, Wang P-Y, Shahsavarani H (2021a) The role of cellulose nanowhiskers in controlling phase segregation, crystallization and thermal stimuli responsiveness in PCL-PEGx-PCL block copolymer-based PU for human tissue engineering applications. Carbohydr Polym 252:117219. https://doi.org/https://doi.org/10.1016/j.carbpol.2020.117219

43. Noormohammadi F, Nourany M, Mir Mohamad Sadeghi G, Wang PY, Shahsavarani H (2021b) The role of cellulose nanowhiskers in controlling phase segregation, crystallization and thermal stimuli responsiveness in PCL-PEGx-PCL block copolymer-based PU for human tissue engineering applications. *Carbohydrate Polymers*, *252*. https://doi.org/10.1016/j.carbpol.2020.117219
44. Nourany M, Ghelichkhani S, Sarkhosh H, Zakizadeh M, Behrouz T (2021) The effect of PCL/PEG ABA block lengths on the crystallization of homo/block- based polyurethane/CNW nanocomposites. J Polym Res 28(1). https://doi.org/10.1007/s10965-020-02376-y
45. Park SH, Oh KW, Kim SH (2013) Reinforcement effect of cellulose nanowhisker on bio-based polyurethane. Compos Sci Technol 86:82–88. https://doi.org/https://doi.org/10.1016/j.compscitech.2013.07.006
46. Parnell S, Min K, Cakmak M (2003) Kinetic studies of polyurethane polymerization with Raman spectroscopy. Polymer 44(18):5137–5144. https://doi.org/https://doi.org/10.1016/S0032-3861(03)00468-3
47. Pei Z, Yu Z, Li M, Bai L, Wang W, Chen H, Yang H, Wei D, Yang L (2021) Self-healing and toughness cellulose nanocrystals nanocomposite hydrogels for strain-sensitive wearable flexible sensor. Int J Biol Macromol 179:324–332. https://doi.org/https://doi.org/10.1016/j.ijbiomac.2021.03.023
48. Prataviera R, Pollet E, Bretas RES, Avérous L, Lucas AA (2018) Nanocomposites based on renewable thermoplastic polyurethane and chemically modified cellulose nanocrystals with improved mechanical properties. J Appl Polym Sci 135(45):46736. https://doi.org/https://doi.org/10.1002/app.46736
49. Qu Q, He J, Da Y, Zhu M, Liu Y, Li X, Tian X, Wang H (2021) High Toughness Polyurethane toward Artificial Muscles, Tuned by Mixing Dynamic Hard Domains. Macromolecules 54(17):8243–8254. https://doi.org/10.1021/acs.macromol.1c01098
50. Rabe M, Verdes D, Seeger S (2011) Understanding protein adsorption phenomena at solid surfaces. Adv Colloid Interface Sci 162(1):87–106. https://doi.org/https://doi.org/10.1016/j.cis.2010.12.007
51. Ranjbar HA, Nourany M, Mollavali M, Noormohammadi F, Jafari S (2021) Stimuli-responsive polyurethane bionanocomposites of poly(ethylene glycol)/poly(ε-caprolactone) and [poly(ε-caprolactone)-grafted-] cellulose nanocrystals. Polym Adv Technol 32(1):76–86. https://doi.org/https://doi.org/10.1002/pat.5062
52. Reid MS, Villalobos M, Cranston ED (2017) Benchmarking Cellulose Nanocrystals: From the Laboratory to Industrial Production. Langmuir 33(7):1583–1598. https://doi.org/10.1021/acs.langmuir.6b03765
53. Roman M, Dong S, Hirani A, Lee YW (2009) Cellulose Nanocrystals for Drug Delivery. In *Polysaccharide Materials: Performance by Design* (Vol. 1017, pp. 4–81). American Chemical Society. https://doi.org/doi:10.1021/bk-2009-1017.ch004
54. Rueda L, Saralegui A, Fernández d'Arlas B, Zhou Q, Berglund LA, Corcuera MA, Mondragon I, Eceiza A (2013) Cellulose nanocrystals/polyurethane nanocomposites. Study from the viewpoint of

microphase separated structure. Carbohydr Polym 92(1):751–757. https://doi.org/https://doi.org/10.1016/j.carbpol.2012.09.093

55. SaifulAzry SOA, Chuah TG, Paridah MT, Aung MM, Ridzuan MA, Lee CH, Sariah S, Lee SH, Juliana AH (2021) Influence of cellulose II polymorph nanowhiskers on bio-based nanocomposite film from Jatropha oil polyurethane. Mater Res Express 8(1):15003. https://doi.org/10.1088/2053-1591/abc6ce
56. Saralegi A, Fernandes SCM, Alonso-Varona A, Palomares T, Foster EJ, Weder C, Eceiza A, Corcuera MA (2013) Shape-Memory Bionanocomposites Based on Chitin Nanocrystals and Thermoplastic Polyurethane with a Highly Crystalline Soft Segment. Biomacromolecules 14(12):4475–4482. https://doi.org/10.1021/bm401385c
57. Sarkhosh H, Nourany M, Noormohammadi F, Ranjbar HA, Zakizadeh M, Javadzadeh M (2021) Development of a semi-crystalline hybrid polyurethane nanocomposites for hMSCs cell culture and evaluation of body- temperature shape memory performance and isothermal crystallization kinetics. J Polym Res 28(5). https://doi.org/10.1007/s10965-021-02522-0
58. Scetta G, Ju J, Selles N, Heuillet P, Ciccotti M, Creton C (2021) Strain induced strengthening of soft thermoplastic polyurethanes under cyclic deformation. J Polym Sci 59(8):685–696. https://doi.org/https://doi.org/10.1002/pol.20210060
59. Shirole A, Nicharat A, Perotto CU, Weder C (2018) Tailoring the Properties of a Shape-Memory Polyurethane via Nanocomposite Formation and Nucleation. Macromolecules 51(5):1841–1849. https://doi.org/10.1021/acs.macromol.7b01728
60. Stribeck N, Li X, Kogut I, Moritz H-U, Eling B, Goerigk GJ, Hoell A (2015) Morphological Failure Mechanisms in Tensile Tests of Crosslinked Polyurethanes With Poorly Developed Domain Structure. Macromol Mater Eng 300(7):699–711. https://doi.org/https://doi.org/10.1002/mame.201500007
61. Tang J, Sisler J, Grishkewich N, Tam KC (2017) Functionalization of cellulose nanocrystals for advanced applications. J Colloid Interface Sci 494:397–409. https://doi.org/https://doi.org/10.1016/j.jcis.2017.01.077
62. Tian D, Wang F, Yang Z, Niu X, Wu Q, Sun P (2019) High-performance polyurethane nanocomposites based on UPy-modified cellulose nanocrystals. Carbohydr Polym 219:191–200. https://doi.org/https://doi.org/10.1016/j.carbpol.2019.05.029
63. Tingaut P, Zimmermann T, Sèbe G (2012) Cellulose nanocrystals and microfibrillated cellulose as building blocks for the design of hierarchical functional materials. J Mater Chem 22(38):20105–20111. https://doi.org/10.1039/C2JM32956E
64. Tito NB, Creton C, Storm C, Ellenbroek WG (2019) Harnessing entropy to enhance toughness in reversibly crosslinked polymer networks. Soft Matter 15(10):2190–2203. https://doi.org/10.1039/C8SM02577K
65. Trache D, Hussin MH, Haafiz MKM, Thakur VK (2017) Recent progress in cellulose nanocrystals: sources and production. Nanoscale 9(5):1763–1786. https://doi.org/10.1039/C6NR09494E

66. Urbina L, Alonso-Varona A, Saralegi A, Palomares T, Eceiza A, Corcuera M, Retegi A (2019) Hybrid and biocompatible cellulose/polyurethane nanocomposites with water-activated shape memory properties. Carbohydr Polym 216:86–96. https://doi.org/https://doi.org/10.1016/j.carbpol.2019.04.010
67. Vanderfleet OM, Cranston ED (2021) Production routes to tailor the performance of cellulose nanocrystals. Nat Reviews Mater 6(2):124–144. https://doi.org/10.1038/s41578-020-00239-y
68. Vilgis T, Halperin A (1991) Aggregation of coil-crystalline block copolymers: equilibrium crystallization. Macromolecules 24(8):2090–2095. https://doi.org/10.1021/ma00008a058
69. Vorov OK, Livesay DR, Jacobs DJ, Science O (2008) *Conformational Entropy of an Ideal Cross-Linking Polymer Chain*. 285–308. https://doi.org/10.3390/e10030285
70. Wang Y-J, Jeng U-S, Hsu S (2018) Biodegradable Water-Based Polyurethane Shape Memory Elastomers for Bone Tissue Engineering. ACS Biomaterials Science & Engineering 4(4):1397–1406. https://doi.org/10.1021/acsbiomaterials.8b00091
71. Wang Y, Cheng Z, Liu Z, Kang H, Liu Y (2018) Cellulose nanofibers/polyurethane shape memory composites with fast water-responsivity. J Mater Chem B 6(11):1668–1677. https://doi.org/10.1039/C7TB03069J
72. Wu H, Xie H, Tian X, Sun Y, Shi B, Zhou Y, Sheng D, Liu X, Yang Y (2021) Hard, tough and fast self-healing thermoplastic polyurethane. Prog Org Coat 159:106409. https://doi.org/https://doi.org/10.1016/j.porgcoat.2021.106409
73. Wu XL, Kang SF, Xu XJ, Xiao F, Ge XL (2014) Effect of the crosslinking density and programming temperature on the shape fixity and shape recovery in epoxy–anhydride shape-memory polymers. J Appl Polym Sci 131(15). https://doi.org/https://doi.org/10.1002/app.40559
74. Xiang N, Zhang X, Zheng M, Xu R, Yan Y (2021) Investigation of tensile behavior and molecular structure of the thermoplastic polyurethane sheets injection molded at different mold temperatures. J Appl Polym Sci 138(38):50959. https://doi.org/https://doi.org/10.1002/app.50959
75. Xie H, Du H, Yang X, Si C (2018) Recent Strategies in Preparation of Cellulose Nanocrystals and Cellulose Nanofibrils Derived from Raw Cellulose Materials. *International Journal of Polymer Science*, *2018*, 7923068. https://doi.org/10.1155/2018/7923068
76. Xiong J, Zheng Z, Jiang H, Ye S, Wang X (2007) Reinforcement of polyurethane composites with an organically modified montmorillonite. Compos Part A: Appl Sci Manufac 38(1):132–137. https://doi.org/https://doi.org/10.1016/j.compositesa.2006.01.014
77. Yu K, Ge Q, Qi HJ (2014) Reduced time as a unified parameter determining fixity and free recovery of shape memory polymers. Nat Commun 5:1–9. https://doi.org/10.1038/ncomms4066
78. Zare M, Prabhakaran MP, Parvin N, Ramakrishna S (2019) Thermally-induced two-way shape memory polymers: Mechanisms, structures, and applications. Chem Eng J 374:706–720. https://doi.org/https://doi.org/10.1016/j.cej.2019.05.167
79. Zeng H, Sun H, Gu J (2021) Modeling the one-way and two-way shape memory effects of semi-crystalline polymers. Smart Mater Struct 30(9):95020. https://doi.org/10.1088/1361-665x/ac179e

80. Zhang K, Zhao Z, Huang J, Zhao T, Fang R, Liu M (2019) Self-recoverable semi-crystalline hydrogels with thermomechanics and shape memory performance. Sci China Mater 62(4):586–596. https://doi.org/10.1007/s40843-018-9347-5
81. Zhang Y, Hu J, Zhao X, Xie R, Qin T, Ji F (2019) Mechanically Robust Shape Memory Polyurethane Nanocomposites for Minimally Invasive Bone Repair. ACS Appl Bio Mater 2(3):1056–1065. https://doi.org/10.1021/acsabm.8b00655
82. Zhou J, Turner SA, Brosnan SM, Li Q, Carrillo J-MY, Nykypanchuk D, Gang O, Ashby VS, Dobrynin AV, Sheiko SS (2014) Shapeshifting: Reversible Shape Memory in Semicrystalline Elastomers. Macromolecules 47(5):1768–1776. https://doi.org/10.1021/ma4023185
83. Zhuravlev E, Schmelzer JWP, Wunderlich B, Schick C (2011) Kinetics of nucleation and crystallization in poly(ε-caprolactone) (PCL). Polymer 52(9):1983–1997. https://doi.org/https://doi.org/10.1016/j.polymer.2011.03.013

Figures

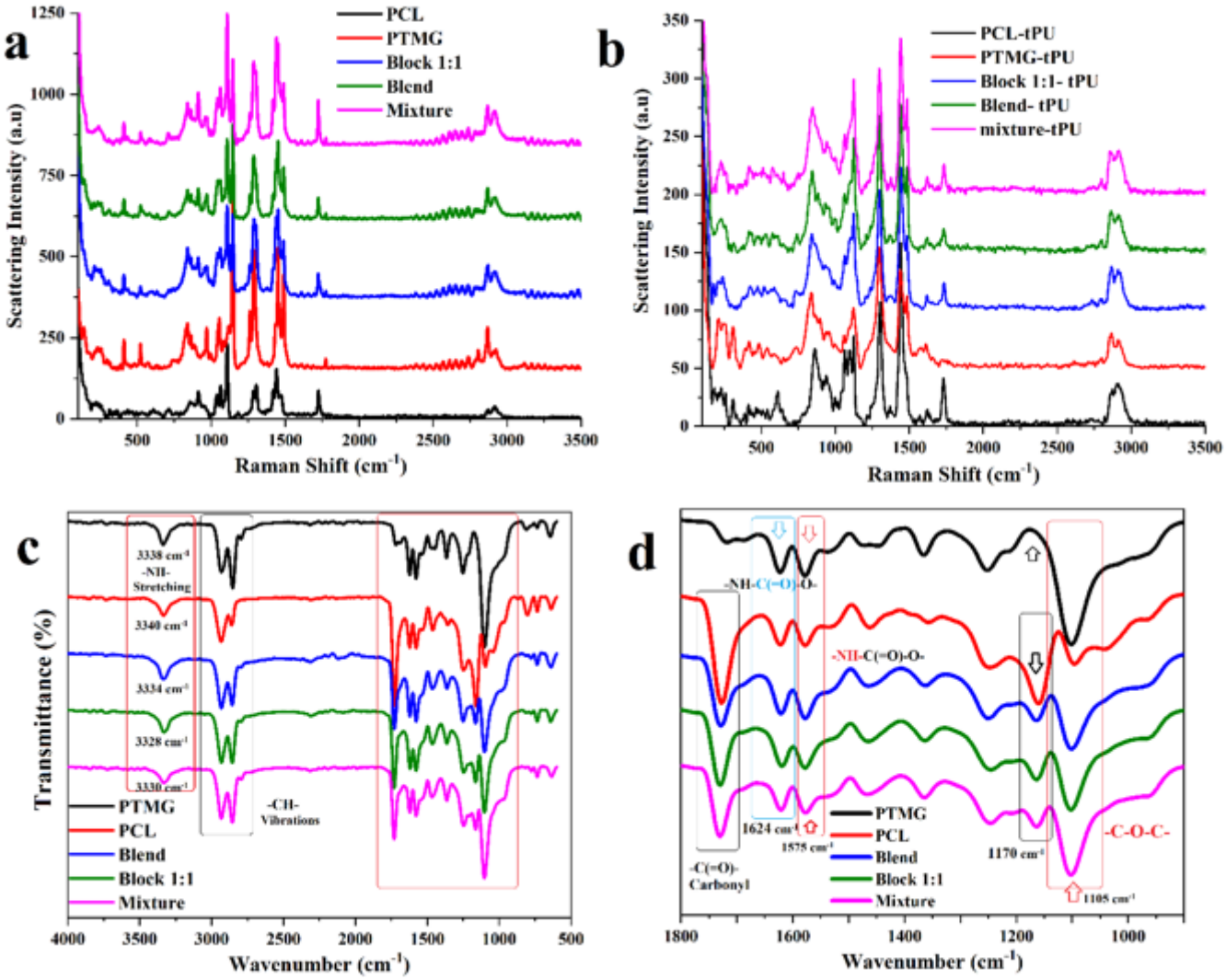

Figure 1

Raman spectroscopy of (a) the polyols and (b) the thermoset PU nanocomposites. (c, d) ATR-FTIR spectrum of the synthesized thermoset PU nanocomposites.

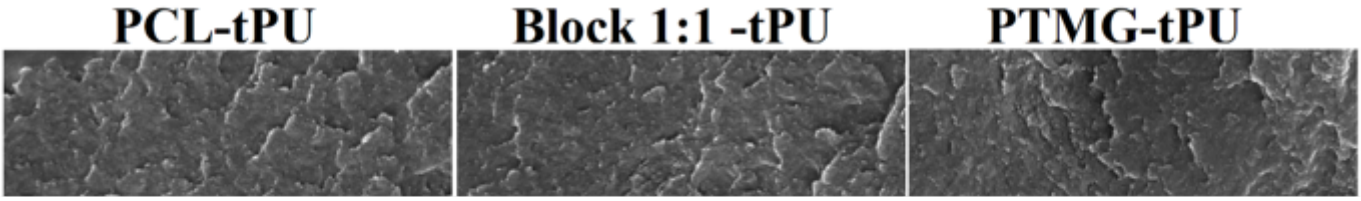

Figure 2

SEM images of PCL-tPU, Block 1:1-tPU, PTMG-tPU: (first row) cross-section images with 5 μm scale, (second row) cross-section images with 1 μm scale and (third row) surface images of the tPUs with 1 μm scale-bar.

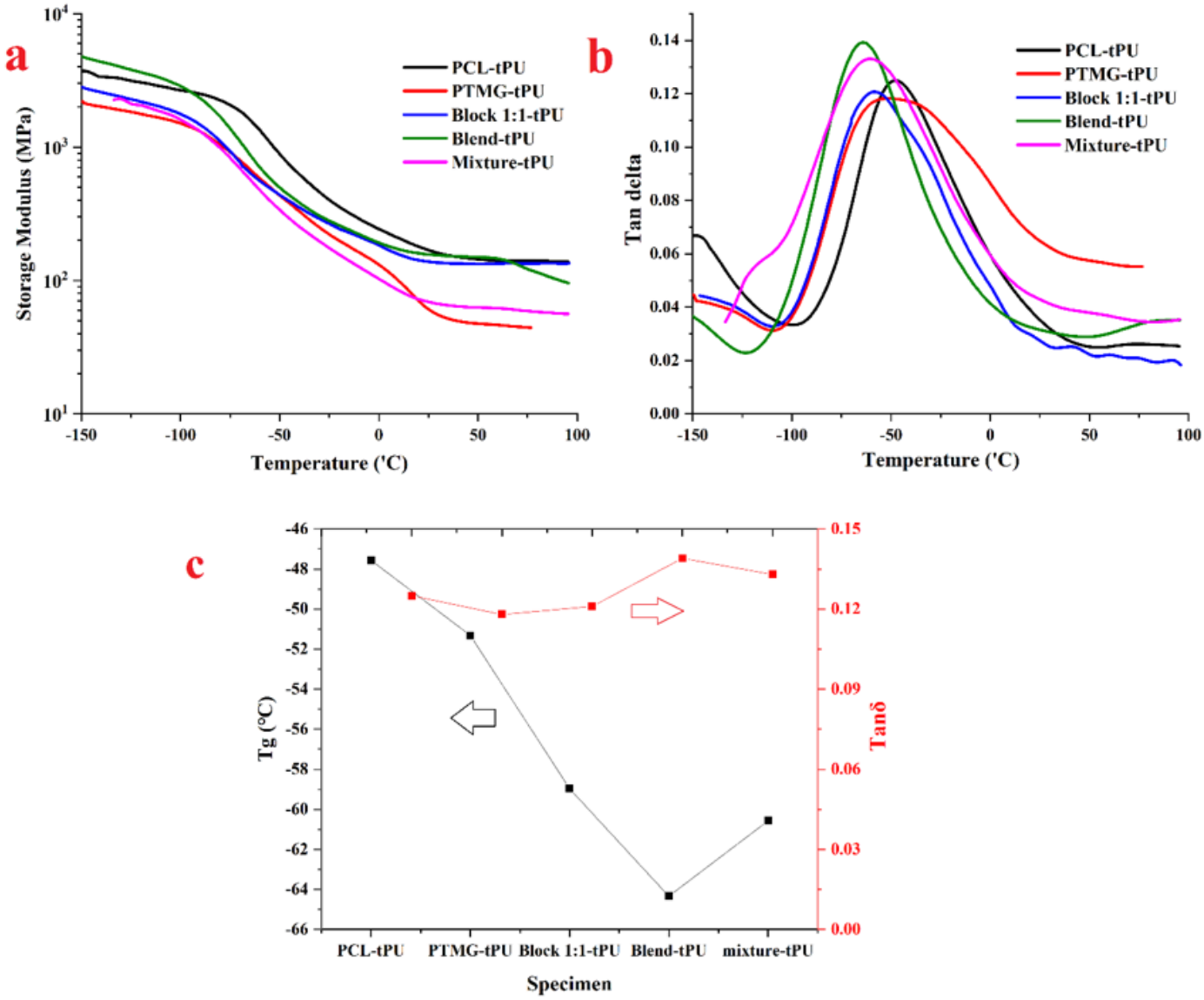

Figure 3

(a) Storage modulus and (b) tanδ vs. temperature of the synthesized tPUs; (c) Tg and tanδ values of the tPUs.

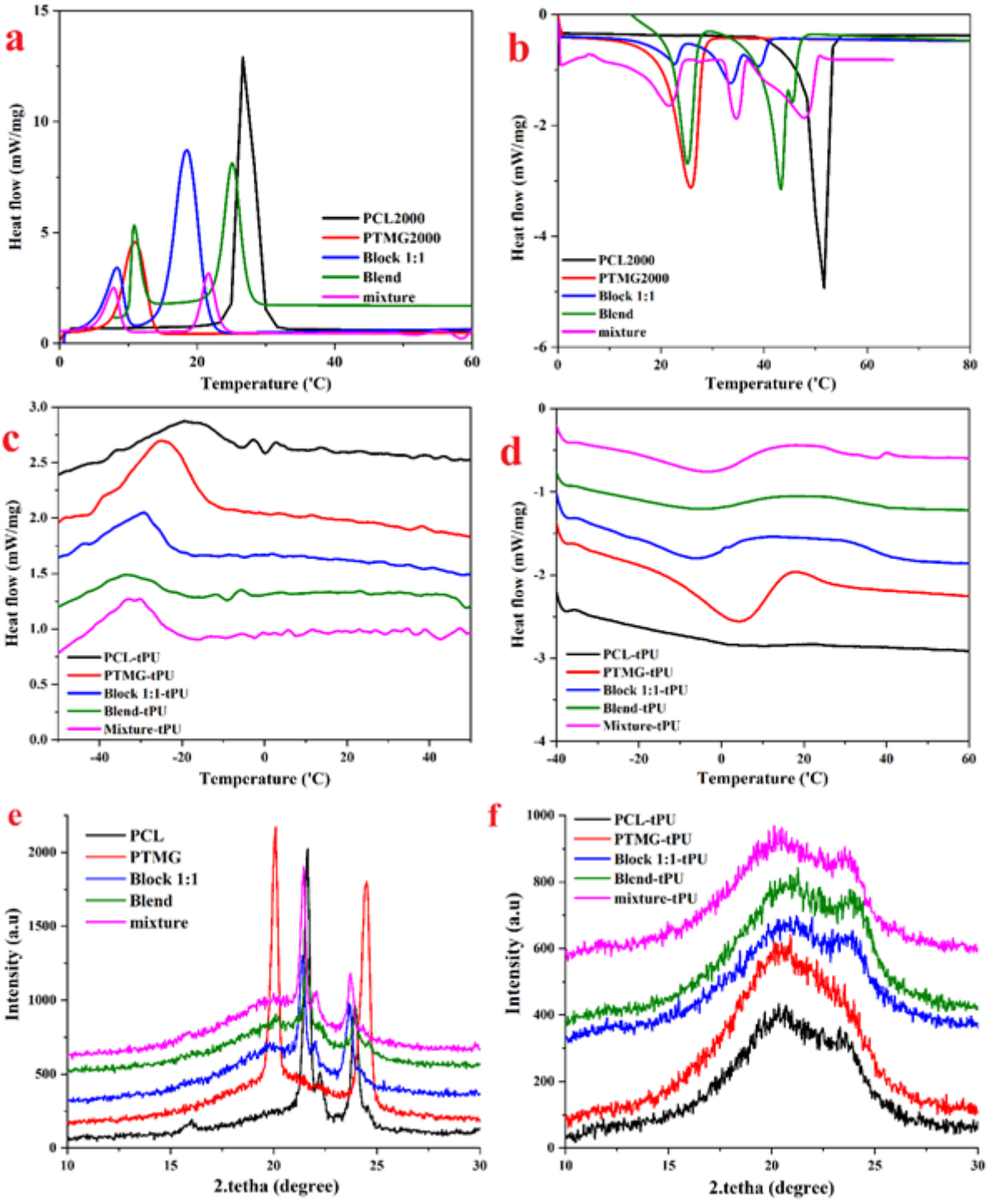

Figure 4

The DSC thermograms of the polyols and the thermoset PUs: (a) second heating and (b) cooling regime of the polyols; (c) second heating and (d) cooling regime of the tPUs. The X-ray diffraction spectrum of (a) the polyols and (b) the thermoset PU/CNW nanocomposites.

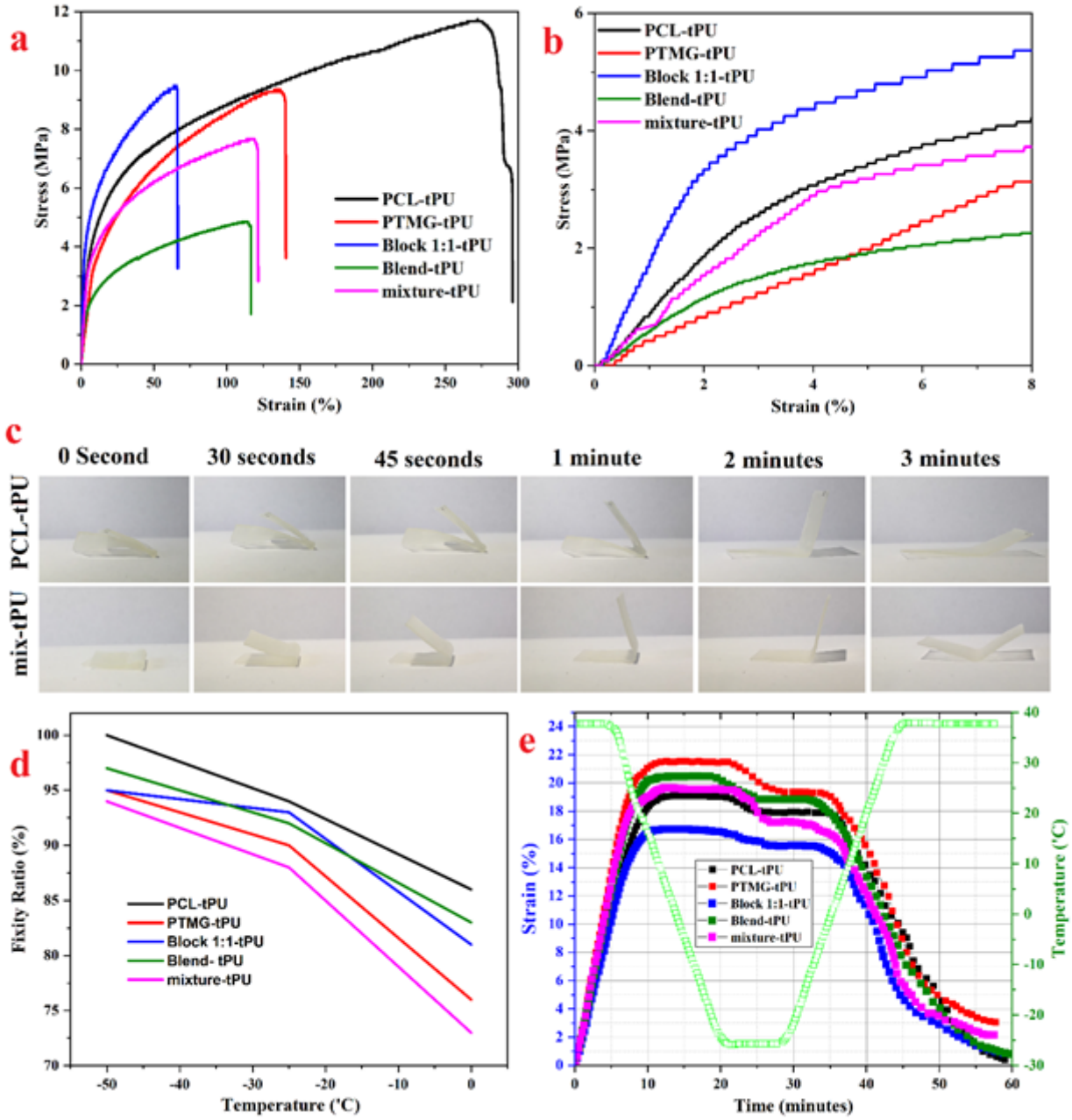

Figure 5

The stress-strain behavior of the thermoset PU/CNW nanocomposites (a) in full-scale and (b) low-strain scale. (c) Digital photographs of the PCL- and mixture-tPUs recovering at room temperature, (d) shape fixity ratio as a function of temperature, and (e) the shape memory process of the thermoset PU nanocomposites fixed at -25 with the recovery temperature of +37.5 .

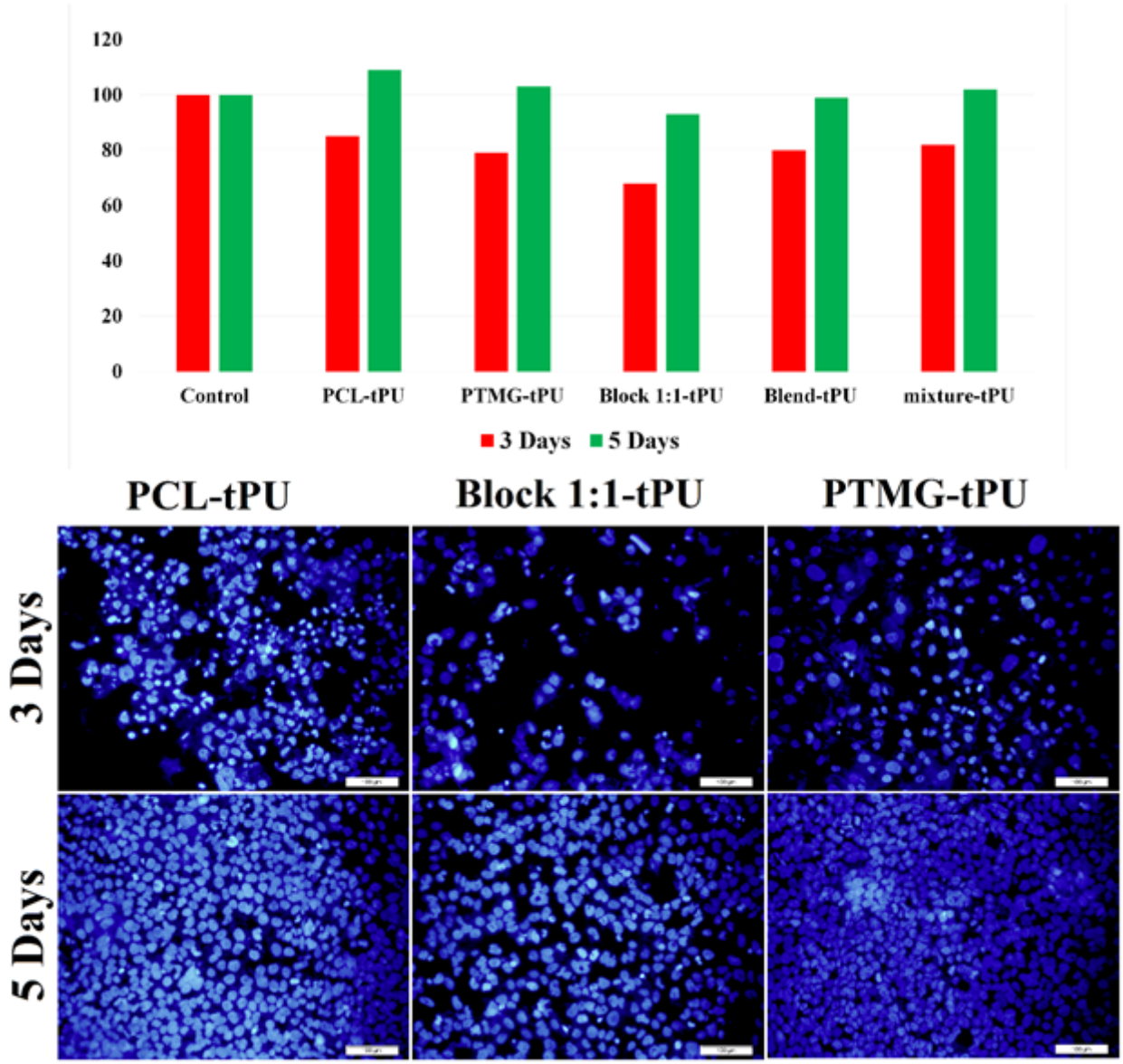

Figure 6

(Top) MTT assay using HFF cells cultured on the thermoset PU/CNW nanocomposites for 3 and 5 days. (Bottom) Fluorescent images of the cell-seeded films after 3 and 5 days of culturing HFF cells.

Supplementary Files

This is a list of supplementary files associated with this preprint. Click to download.

- GraphicalImage.png